

# Co-Segmentation of Pheochromocytomas in CECT Images

Greeshma H

Dept.of Electronics and Communication  
Younus College of Engineering and technology  
Kollam, India

Nishil A

Assistant Professor  
Dept.of Electronics and Communication  
Younus College of Engineering and technology  
Kollam, India

**Abstract**—Segmentation of pheochromocytomas in Contrast-Enhanced Computed Tomography (CECT) images is an ill-posed problem due to the presence of weak boundaries, intratumoral degeneration, and nearby structures and clutter. Additional information from different phases of CECT images needs to be imposed for better mass segmentations. A novel co-segmentation method is proposed by incorporating a localized region-based level set model (LRLSM). The energy function is formulated with consideration of adaptive tradeoff between the complementary local information from image. Gradient direction and shape dissimilarity measure are integrated to guide the level set evolution. Automatic localization radius selection is added to further facilitate the segmentation.

**Index Terms**—localized energy, contrast-enhanced computed tomography (CECT), co-segmentation, level set model, pheochromocytoma.

## I. INTRODUCTION

Pheochromocytomas are tumors arising from chromaffin tissue of the adrenal medulla or extra-adrenal paraganglia. Although in general, the prevalence of pheochromocytomas in outpatient clinics is low the potent effects of secreted catecholamines lead to serious and potentially life-threatening cardiovascular complications. Accounting for about 10% of masses are malignant that need radical surgical removal of tumor tissue. Correct and noninvasive characterization of pheochromocytomas is of critical importance because any handling of these masses can precipitate a hypertensive crisis. Imaging techniques like Ultrasound, Computed Tomography (CT), Magnetic Resonance (MR) and Functional Imaging have been shown to be useful. Especially, CT is preeminent in adrenal imaging and most pheochromocytomas are detected during CT scanning with and without contrast.

Contrast-enhanced CT (CECT) is a primary imaging modality for its ability to differentiate two types of adrenal tumors: pheochromocytoma and adrenal adenoma, which are difficult to be distinguished in an unenhanced CT image. Besides, small pheochromocytomas tend to be solid and large ones contain various forms of intratumoral degeneration, such as cystic changes, necrosis, hemorrhage and calcifications. CECT scans produce a better diagnosis by displaying distinct attenuation values to different types of degeneration. In clinical practice, a CECT usually has two phases, the arterial phase (AP) and the portal-venous phase (PP). PP images are typically acquired 30 seconds after AP. As a result of temporally varying proportions of

contrast medium, pheochromocytomas and surrounding abdominal structures exhibit dissimilar density distributions between AP and PP images. To inspect pheochromocytomas, urologists commonly combine detailed and complementary anatomical image information at different phases

## II. LITERATURE SURVEY

Mass characterization plays a significant role in the diagnosis, prognosis and treatment of pheochromocytomas. The characterization primarily relies on the assessment of attenuation values and density heterogeneity [4], [8]. Accurate tumor segmentation and precisely delineated contours are the prerequisite for quantitative measurements. In clinical applications, the contours of pheochromocytomas in CECT images at AP and PP are manually drawn by experts [5]-[7]. However, manual segmentation is time-consuming, subjective and highly dependent on the experts' experience. When masses compress surrounding organs, blurred or missing boundaries may lead to manual errors. Moreover, various types of intratumoral degeneration and surrounding clutter give rise to complex foreground and background that complicate the delineation. Automated or semi-automated segmentation methods would have improvements in efficiency and accuracy. Computer-aided CT tumor segmentation has become an active field of research. Methods are mainly divided into three groups: graph-based, learning-based and deformable models. Graph cuts methods are employed for either initial liver segmentation or hepatic tumors using constraints such as shape and enhancement [9], [10]. However, the heterogeneity of large masses and the partial volume effect of CT imaging severely affect the performance of graph-based methods. Machine learning techniques are introduced to the classification of tumors and healthy tissues as well as different types of lesions [11], [12]. Learning-based methods allow the usage of high-dimensional features to achieve a better discriminatory power, whereas the spatial correlation between pixels is hardly considered. To complement the drawbacks, Keshani *et al.* combined an active contour model (ACM) for accurate segmentation of lung nodules [13]. Including ACM, deformable models are influential and successful in the CT tumor segmentation. Especially, level set models (LSMs) embedding the dynamic curves and surfaces are advantageous to represent complex topology and handle topological changes [14].

### III. PROPOSED MEHOD

The proposed method is applied to the pheochromocytoma co-segmentation in CECT image pairs. Our method has three steps: initialization, co-segmentation level set formulation and energy function minimization. The details are described in the following sections.

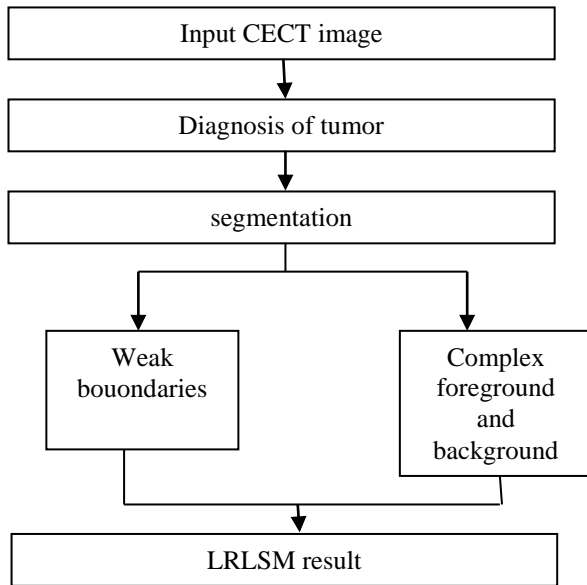


Fig 1. Block diagram of proposed mehod

#### A. Initialization

The input is a given image  $I^k, k \in \{0,1\}$ , of the same pheochromocytoma at AP or PP. Because patients are informed with breath-holding requirements during image acquisition, the mass at different phases present slight differences. Compared to other organs, pheochromocytomas are much smaller and the difference often could be neglected. Either one in the AP or PP image can be the basic of the initialization. The user simply needs to place three points to define an ellipse which is regarded as the initial contour. One point is placed near the center of the mass and the other two points are placed to approximate the endpoints of the major and minor axes.

#### B. Co-segmentation Level Set Formulation

To incorporate the co-segmentation into the LRLSM framework, LSFs  $\phi^k$  corresponding to  $I^k$  are generated from the same initial contour. Based on the initial contour, localization radius is automatically chosen to reduce the user interaction. In the co-segmentation process, each LSF is evolved based on the local statistics of the image and the constraint of the other LSF. For image  $I^k$  of each image, a new energy function is proposed.

$$E(\phi^k) = \lambda_i^k \cdot \text{Length}(\phi^k) + \lambda_s^k \cdot \text{Shape}(\phi^k, \phi^{1-k}) + \int_{\Omega} \delta \phi^k(x) [\lambda_i^k f^L(I^k, \phi^k, r^k) + \lambda_0^k f^L(I^{1-k}, \phi^k, r^{1-k})] dx \quad (1)$$

The novel  $f^L(I^{1-k}, \phi^k, r^{1-k})$  represents local statistics inside and outside the evolving zero level set of LSF  $\phi^k$  on

the other image  $I^{1-k}$  of the image pair. Hence, localized energies of each image pair  $I^k$  and  $I^{1-k}$  are integrated to guide the evolution of  $\phi^k$ . Moreover, the shape term  $\text{Shape}(\phi^k, \phi^{1-k})$  is introduced to penalize the dissimilarity between the two LSFs  $\phi^k$  and  $\phi^{1-k}$  along the co-segmentation process. Therefore, the complementary image information, such as boundary, location and shape, are utilized.

Furthermore, unlike the global region-based flow of existing co-segmentation LSMs, the proposed energy function enforces the use of local image data in the pheochromocytoma segmentation. The LRLSM is integrated for not only its capability to keep the zero level set from boundary leakage in the cases with weak edges, but also its advantage in the cases with density inhomogeneity. To flexibly utilize the LRLSM, the sum of two localized region-based energies from the image pair is calculated under the adaptive weights  $\lambda_i^k$  and  $\lambda_0^k$ . In addition, the gradient direction is incorporated into the length term  $\text{Length}(\phi^k)$  to evolve the zero level set to converge to the object boundaries.

#### 1) Length term and gradient direction

Clinical studies shows that pheochromocytomas present inhomogeneous density levels. Intratumoral degeneration forms the hole and results in inner edges. Surrounding tissues and organs may close or even be compressed by masses, which leads to ambiguous boundaries. To avoid being attracted to undesired edges, we integrate the gradient direction into the level set framework. A general edge-detector with respect to the image gradient can be defined by a positive and decreasing function. The edge-detector function  $g$  has the low value close to zero at edges while indicates the high value close to 1 in homogeneous regions.

#### 2) Shape term

Pheochromocytoma in each image pair has similarity with respect to the shape and the location. To penalize the difference between two zero LSFs, we exploit two Heaviside functions as a dissimilarity measure of two shape representations. The shape dissimilarity measure is defined as

$$\text{Shape}(\phi^k, \phi^{1-k}) = \int [H\phi^k(x)(1 - H\phi^{1-k}(x)) + H\phi^{1-k}(x)(H\phi^k(x))] dx \quad (2)$$

where  $\text{Shape}(\phi^k, \phi^{1-k})$  denotes the disagreement between the classifications of the foreground and background in the image pair, the foreground and background in image  $I^k$  are labeled by  $H\phi^k$  and  $(1 - H\phi^k)$  respectively, and those of the other image  $I^{1-k}$  are indicated by  $H\phi^{1-k}$  and  $(1 - H\phi^{1-k})$  respectively. In our method, the co-segmentation is done through a mutual procedure in which two LSFs are evolved and refined alternately. In other words, only the segmenting zero level set is evolved on each iteration, and the other LSF is employed as a dynamic shape prior.

#### 3) Automated selection of localization radius

The localization radius  $r$  in the LRLSM is manually selected by the user based on the proximity of the scale of the object and the presence of the nearby clutter

.Herein, we introduce an automated way that makes use of the initial contour to approximate the size of the tumor and the presence of surrounding clutter. For image  $I^k$ , the value of localization radius is set as:

$$r^k = \text{round}(\sqrt{S/2(v^k+1)}) \quad (3)$$

where  $r^k$  is the localization radius,  $S$  denotes the area covered by the initial contour,  $v^k$  corresponding to  $I^k$  depicts the local variation ratio, two constants 2 and 1 guarantee  $r^k$  to be in a rational range, that is 5 to 15 pixels for most cases. The local variation ratio  $v^k$  is defined as:

$$v^k = \text{mean}((\exp(\text{var}(y_0)/\text{mean}(y_0)^2)) \quad (4)$$

where  $x_0$  is the pixel on the initial contour  $C_0$ ,  $y_0$  is the pixel falling into the localization ball  $B_0(x_0, y_0)$  centered at  $x_0$  of initial radius  $r_0 = 10$  pixels.

The initial contour lies not far away from the pheochromocytoma boundaries. Hence, the value of  $S$  is able to approximate the mass size. The value of  $V^k$  reflects the homogeneity degree of local regions along the initial contour and estimates the presence of nearby clutter. It has small values in homogeneous regions and produces large values at edges or in the local regions corrupted by the clutter. Therefore, a large radius  $r^k$  is defined in the case of a large mass with homogeneous boundaries whereas small radii are chosen in the cases of small masses having surrounding clutter.

### C. Energy Function Minimization

The co-segmentation energy function is expressed as :

$$E(\phi^k) = \lambda_1 \int_{\Omega} g^k \delta(\phi^k(x)) |\nabla \phi(x)| dx + \lambda_s \int_{\Omega} [H\phi^k(x)(1-H\phi^{1-k}(x)) + H\phi^{1-k}(x)(1-H\phi^k(x))] dx + \int_{\Omega} \delta\phi^k(x)(1-\omega^k) f^L(I^k, \phi^k, r^k) + \omega^k f^L(I^{1-k}, \phi^k, r^{1-k}) dx \quad (5)$$

By taking the first variation with respect to  $\phi^k$ , we obtain the evolution equation represented as

$$\partial\phi / \partial t = \delta\phi^k(x) [\lambda_1 \text{div}^k(\nabla\phi(x)/|\nabla\phi(x)|) + \lambda_s(2H\phi^{1-k}(x)-1) + (1-\omega^k)\nabla f^L(I^k, \phi^k, r^k) + \omega^k \nabla f^L(I^{1-k}, \phi^k, r^{1-k})] \quad (6)$$

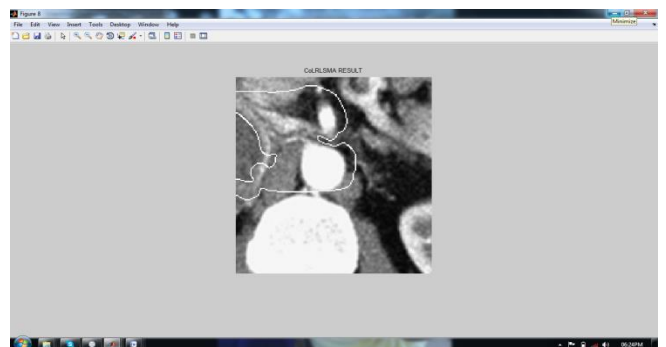
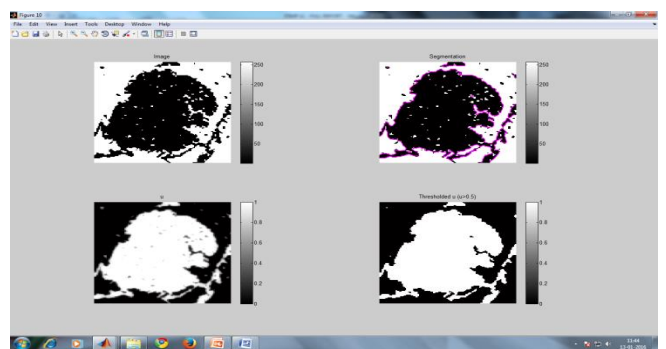
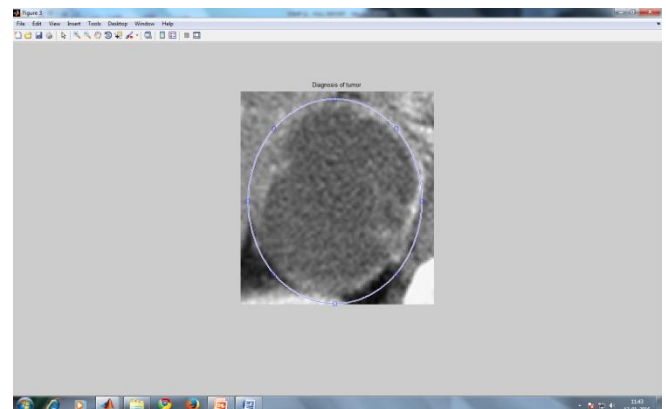
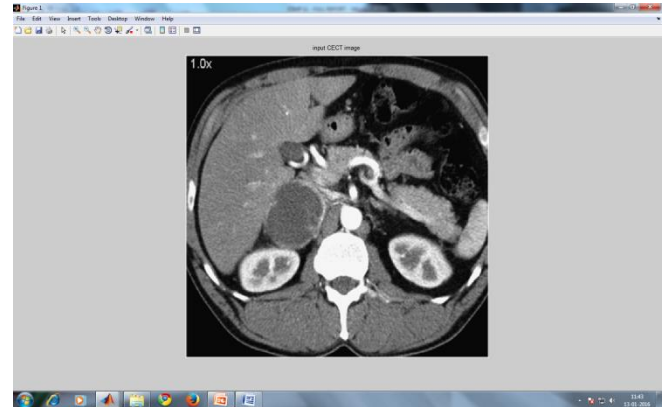
LSFs corresponding to the image pair are evolved and refined alternately by minimizing the co-segmentation energy function. The evolution of LSF is based on the data of the image pair. Besides, a new convergence test is introduced to stop the iteration process once the desired contours are obtained.

## IV. EXPERIMENTAL RESULTS

Though patients are instructed to hold their breath during CT scanning, images may still exhibit slight difference at two phases. To verify that choosing the AP or PP image for initialization were both feasible, different forms of initial contour placement were conducted.

The ground truth is initialized with complexed foreground and background image. The same initial contour for all test algorithms was depicted. Hence, proposed method performed consistently well in the case with complex foreground and background. The efficiency and minimum operator interaction were highly valued in

clinical practice. This method merely required the user to set points to define an ellipse as the initial contour. The initialization method is simple and feasible and highly reduces the manual labor for physicians. Afterwards, there was no operator interaction for the co-segmentation in images.



## V. CONCLUSION.

A novel LRLSM-based method to the pheochromocytoma co-segmentation in CECT images. The energy function is formulated from the localized energies from images. Gradient direction, shape dissimilarity measure and automated localization radius selection are integrated to further facilitate the segmentation. Then, LSFs are evolved and refined alternately through a mutual procedure to achieve the energy function minimization. By taking advantage of the local-region based complementary information from image pairs, the proposed method performed consistently well in the cases with weak boundaries and complex foreground and background.

In clinical practice, accurate manual segmentation and measurements of pheochromocytomas rely on referencing of relevant image data from multiple phases and also adjacent slices. Improvements will be the use of information from image sequences or volumes, such as 3-D pheochromocytoma segmentation. Automatic detection and segmentation of pheochromocytomas will further elevate the efficiency. Based on the proposed co-segmentation method, future work will be extension to applications of other tumors at different phases.

## ACKNOWLEDGMENT

The author thankfully acknowledges Mr. Nishil Assistant Professor, YCE, without whose guidance and supervision, this work would not been possible. I would like to extend my gratitude to the Head of the Department of Electronics and Communication Mr. Rajeev S K who were always ready to help me with ideas and suggestions for rectifying the mistakes that crept up time to time during the completion of this venture. I would also like to thank my friends and last but not least the staff of ECE department for their whole hearted support and encouragement. Above all, I am thankful to the God almighty.

## REFERENCES

- [1] J. W. Lenders, G. Eisenhofer, M. Mannelli, and K. Pacak, "Pheochromocytoma," *Lancet*, vol. 366, no. 9486, pp. 665-675, Aug. 2005.
- [2] A. Tsirlin, Y. Oo, R. Sharma, A. Kansara, A. Gliwa, and M. A. Banerji, "Pheochromocytoma: a review," *Maturitas*, vol. 77, no. 3, pp. 229-238, Mar. 2014.
- [3] K. Leung, M. Stamm, A. Raja, and G. Low, "Pheochromocytoma: the range of appearances on ultrasound, CT, MRI, and functional imaging," *AJR*, vol. 200, no.2, pp. 370-378, 2013.
- [4] M. A. Blake, S. K. Krishnamoorthy, G. W. Boland, A. T. Sweeney, M. B. Pitman, M. Harisinghani, P. R. Mueller, and P. F. Hahn, "Low-density pheochromocytoma on CT: a mimicker of adrenal adenoma," *AJR*, vol. 181, no. 6, pp. 1663-1668, Dec. 2003.
- [5] A. M. Halefoglul, N. Bas, A. Yasar, and M. Basak, "Differentiation of adrenal adenomas from nonadenomas using CT histogram analysis method: a prospective study," *Eur. J. Radiol.*, vol. 73, no. 3, pp. 643-651, Mar. 2010.
- [6] D. H. Szolar, M. Korobkin, P. Reittner, A. Berghold, T. Bauernhofer, H. Trummer, H. Schoellnast, K. W. Preidler, and H. Samonigg, "Adrenocortical carcinomas and adrenal pheochromocytomas: mass and enhancement loss evaluation at delayed contrast-enhanced CT," *Radiol.*, vol. 234, no.2, pp. 479-485, Feb. 2005.
- [7] G. A. Motta-Ramirez, E. M. Remer, B. R. Herts, I. S. Gill, and A. H. Hamrahian, "Comparison of CT findings in symptomatic and incidentally discovered pheochromocytomas," *AJR*, vol. 185, no.3, pp. 684-688, Sep. 2005.
- [8] J. Patel, M. S. Davenport, R. H. Cohan, and E. M. Caoili, "Can established CT attenuation and washout criteria for adrenal adenoma accurately exclude pheochromocytoma?," *AJR*, vol. 201, no. 1, pp. 122-127, Jul. 2013.
- [9] R. Beichel, A. Bornik, C. Bauer, and E. Sorantin, "Liver segmentation in contrast enhanced CT data using graph cuts and interactive 3D segmentation refinement methods," *Med. phys.*, vol. 39, no. 3, pp. 1361-1373, 2012.
- [10] M. G. Linguraru, W. J. Richbourg, J. Liu, J. M. Watt, V. Pamulapati, S. and Wang, R. M. Summers, "Tumor burden analysis from CT data of diseased patients via automated liver and tumor segmentation," *IEEE Trans. Med. Imag.*, vol. 31, no. 10, pp. 1965-1976, Oct. 2012.
- [11] M. Freiman, O. Cooper, D. Lischinski, and L. Joskowicz, "Liver tumors segmentation from CTA images using voxels classification and affinity constraint propagation," *Int. J. Comput. Assist. Radiol. Surg.*, vol.6, no. 2, pp. 247-255, Mar. 2011.
- [12] F. Zhang, Y. Song, W. Cai, M. Lee, Y. Zhou, H. Huang, S. Shan, M. J. Fulham, and D. D. Feng, "Lung nodule classification with multi-level patch-based context analysis," *IEEE Trans. Biomed. Eng.*, vol. 61, no. 4, pp. 1155-1166, Apr. 2014.
- [13] M. Keshani, Z. Azimifar, F. Tajeripour, and R. Boostani, "Lung nodule segmentation and recognition using SVM classifier and active contour modeling: a complete intelligent system," *Comput. Biol. Med.*, vol. 43, no. 4, pp. 287-300, May 2013.
- [14] S. Osher, and J. A. Sethian, "Fronts propagating with curvature-dependent speed: algorithms based on Hamilton-Jacobi formulations," *J. Comput. phys.*, vol. 79, no. 1, pp. 12-49, Nov. 1988.
- [15] R. Tsai, and S. Osher, "Level set methods and their applications in image science," *Commun. Math. Sci.*, vol. 1, no. 4, pp. 1-20, Nov. 2003.
- [16] M. Kass, A. Witkin, and D. Terzopoulos, "Snakes: active contour models," *Int. J. Comput. Vis.*, vol. 1, no. 4, pp. 321-331, Jan. 1988.
- [17] V. Caselles, R. Kimmel, and G. Sapiro, "Geodesic active contours," *Int. J. Comput. Vis.*, vol. 22, no. 1, pp. 61-79, Feb. 1997.
- [18] N. Paragios, and R. Deriche, "Geodesic active contours and level sets for the detection and tracking of moving objects," *IEEE Trans. Pattern Anal. Mach. Intell.*, vol 22, no. 3, pp. 266-280, Mar. 2000.
- [19] C. Li, C. Xu, C. Gui, and M. D. Fox, "Distance regularized level set evolution and its application to image segmentation," *IEEE Trans. Image Process.*, vol. 19, no.12, pp. 3243-3254, Dec. 2010.
- [20] D. Mumford, and J. Shah, "Optimal approximations by piecewise smooth functions and associated variational problems," *Commun. Pur. Appl. Math.*, vol. 42, no. 5, pp. 577-685, Jul. 1989.
- [21] T. F. Chan, and L. A. Vese, "Active contours without edges," *IEEE Trans. Image Process.*, vol. 10, no. 2, pp. 266-277, Feb. 2001.
- [22] C. Li, C. Y. Kao, J. C. Gore, and Z. Ding, "Implicit active contours driven by local binary fitting energy," *Proc. IEEE CVPR*, pp. 1-7, Jun. 2007.